

## THE FAN OBSERVATORY BENCH OPTICAL SPECTROGRAPH (FOBOS)

JEFFREY D. CRANE, STEVEN R. MAJEWSKI, RICHARD J. PATTERSON, MICHAEL F. SKRUTSKIE, ELENA Y. ADAMS, AND  
PETER M. FRINCHABOY

Department of Astronomy, University of Virginia, Charlottesville, VA 22903

*Accepted for publication in the May 2005 issue of the PASP*

### ABSTRACT

The Fan Observatory Bench Optical Spectrograph (FOBOS) is intended for single-object optical spectroscopy at moderate resolution ( $R \sim 1500 - 3000$ ) using a fiber-fed, bench-mounted design to maintain stability. Whenever possible, the instrument uses off-the-shelf components to maintain a modest cost. FOBOS supports Galactic astronomy projects that require consistently well-measured ( $\sim 5 \text{ km sec}^{-1}$ ) radial velocities for large numbers of broadly distributed and relatively bright ( $V \lesssim 14$ ) stars. The spectrograph provides wavelength coverage throughout the optical spectrum, although the instrument design was optimized for use in the range  $4700 < \lambda < 6700 \text{ \AA}$ . Test data indicate that the instrument is stable and capable of measuring radial velocities with precision better than  $3 \text{ km sec}^{-1}$  at a resolution of  $R \sim 1500$  with minimal calibration overhead.

*Subject headings:* instrumentation: spectrographs, techniques: radial velocities

### 1. INTRODUCTION

The Fan Observatory Bench Optical Spectrograph (FOBOS) addresses an increasing need for efficient moderate-resolution radial velocity surveys of bright stars distributed widely over the sky. As one example, the Grid Giant Star Survey (GGSS; Patterson et al. 2001) for NASA's *Space Interferometry Mission (SIM)* requires spectroscopic study of several thousand bright ( $V < 13.5$ ) K giants evenly spaced about the sky, necessitating large amounts of observing time on small aperture telescopes with single-object spectrographs. Few publicly available facilities with these capabilities exist, especially in the northern hemisphere. In the southern hemisphere, the GGSS had used generous allocations of Las Campanas Observatory (LCO) Swope 1-meter time with the Modular Spectrograph, but this observing mode has since been decommissioned<sup>1</sup>. Moreover, the available facilities are predominantly slit spectrographs.

Slit spectrographs suffer from both mechanical flexure and slit-centroiding errors that result in reduced velocity precision. Seeing can also produce variable spectral resolution. Frequent lamp calibration can reduce flexure errors, but adds substantial overhead. A fiber-fed, bench-mounted spectrograph can mitigate all of these problems, but with a penalty in system throughput. The benefits of stability and ease of use, however, can outweigh the decreased efficiency, particularly when targets are bright and observing time is plentiful. Separating the spectrograph from the telescope also protects the optics from environmental fluctuations (significant in central Virginia) and negates the requirement to fold the optical path into a compact unit mounted on the telescope.

The University of Virginia operates several telescopes at the Fan Mountain Observatory (FMO) in southern Albemarle County, Virginia. The 40 inch telescope is an f/13.5 astrometric reflector with a  $15.0'' \text{ mm}^{-1}$

plate scale originally designed to continue the University's long-running astrometry program with the Leander McCormick Observatory 26 $\frac{1}{4}$ -inch refractor after Charlottesville lights made work there difficult. Following construction in 1970, the 40-inch telescope collected photographic plates for parallaxes. In the 1980's and 1990's, photographic plates gave way to electronic detectors for astrometry and more general photometric imaging, but the astrometry program switched focus to the southern hemisphere (e.g., Patterson & Ianna 1991). The telescope has never been used for research quality spectroscopic work, although the site is perhaps better suited to that purpose (many nights each year are not photometric, but still clear enough to allow spectroscopic observing).

The proximity of the FMO site to the Department of Astronomy, the virtually unlimited availability of observing time, and the good match of aperture size to several survey projects under consideration led to a proposal to build a fiber-fed optical spectrograph for the 40 inch telescope. This proposal for an instrument of modest cost was also supported by the *SIM* project, which had interests in the GGSS expanding to the northern hemisphere. The instrument achieved first light in September 2003. In this paper, we discuss the philosophy, hardware specifications and goals, overall design, construction, and performance of FOBOS and give a brief overview of some of the planned science.

### 2. GOALS AND SPECIFICATIONS

FOBOS was designed primarily to provide northern hemisphere moderate resolution spectroscopy for the GGSS. Since the southern hemisphere GGSS spectroscopic campaign had already commenced on the 1-meter Swope telescope, the original goals for FOBOS were set simply to match the capabilities provided by the LCO Modular Spectrograph on that telescope. Specifically, the observed wavelength range was  $4700 < \lambda < 6700 \text{ \AA}$  and the resolution aimed at  $\sim 10 \text{ km s}^{-1}$  radial velocity accuracy. The purpose of the moderate resolution GGSS spectroscopy was to verify that the photometrically selected giant candidates were in fact giant stars (based on

Electronic address: crane@ociw.edu, srm4n@virginia.edu, rjp0i@virginia.edu, mfs4n@virginia.edu, eys5d@virginia.edu, pmf8b@virginia.edu

<sup>1</sup> Low resolution spectroscopy is, however, still available in the South on the CTIO 1.5-meter telescope.

the  $Mgb+MgH$ ,  $H\beta$ ,  $H\alpha$ , and  $NaD$  lines), and to derive their metallicities, since low abundance giants are preferred for the *SIM* grid. The addition of  $10 \text{ km sec}^{-1}$  velocities make the GGSS sample interesting for studies of Galactic dynamics. GGSS targets are brighter than  $V \sim 13.5$ , so a faint magnitude goal of  $V = 14$  was the primary specification, with the hope of achieving signal to noise ratios (S/N) of  $\sim 20$  at that magnitude in reasonable (10–15 minute) exposures. Care was taken throughout the design process to make choices that would limit light losses and maximize efficiency.

A limited hardware budget drove a design that maximized use of off-the-shelf components. Access to an existing CCD and control electronics, a SITE 2048 $\times$ 2048 CCD with  $24\mu\text{m}$  pixels, helped greatly to minimize cost, but also imposed constraints on the end of the optical train since the CCD was already fixed in a dewar with an unmodifiable back focus. At the front end of the optical path, the telescope’s  $f/13.5$  optics guided the choice of optical fiber diameter, while the telescope back focus afforded by the Cassegrain instrument mount restricted both the position of the fibers and the options regarding target acquisition systems.

### 3. DESIGN

Here we detail our solution to the described goals and constraints, a design that performs to specifications at a net expense of  $< \$35,000$ , less CCD and manpower costs, but including a new spectrograph enclosure within the observatory building.

For the purpose of discussing instrument design and functionality, FOBOS can be separated into three main components. These are (1) the focal plane module, which both provides a mechanism for aligning a target on an optical fiber and houses the calibration lamp assembly, (2) the fiber train, which transmits light from the telescope to the optical bench, and (3) the bench spectrograph itself, where spectral dispersion and data collection occur (Fig. 1). In addition to these components, an enclosure has been constructed to allow for more careful monitoring and control of the environment surrounding the bench spectrograph optics.

#### 3.1. The Focal Plane Module

The focal plane module (Fig. 2) mounts to the base of the telescope at the Cassegrain focus. A movable fold mirror carriage within the module just above the telescope’s focal plane enables three separate optical paths to fulfill three required functions.

##### 3.1.1. Focal Plane Viewing and Target Acquisition

In the first fold mirror position, coarse target acquisition takes place. The telescope image plane is demagnified five times by a system of two achromatic doublet lenses and viewed by a Santa Barbara Instrument Group (SBIG) model STV digital integrating video camera, yielding a  $6.0 \times 4.4$  arcmin field of view. The target star can be viewed, identified, and roughly positioned on the fiber by moving the telescope until the image of the star on a TV monitor is coincident with the known location of the fiber when the fold mirror is retracted. The fiber ends themselves cannot be seen with the STV camera because they lie beneath the fold mirror when the

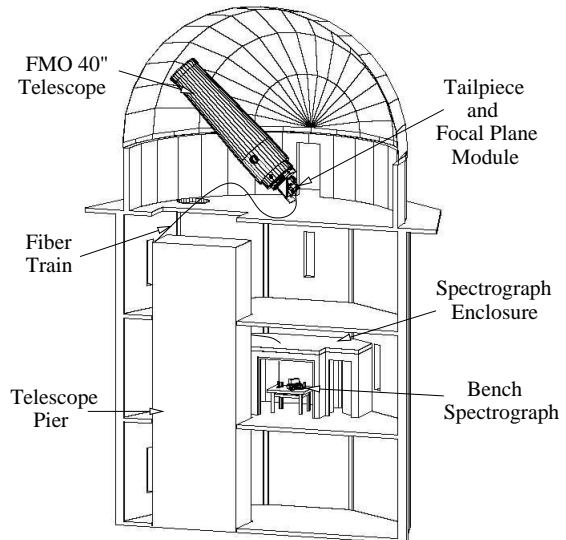


FIG. 1.— The complete FOBOS system on the FMO 40-inch telescope. The building and telescope pier are shown in cross-section. The fiber train runs from the focal plane module through the telescope’s polar axis (not shown) and down the side of the telescope pier to the bench spectrograph enclosure. The enclosure is shown with part of one wall removed.

carriage is in this position. It is also in this position that the telescope focus is adjusted. Relative to the movable fold mirror, the distances to the primary acquisition object plane and to the optical fiber array are equal, so that bringing into focus the image shown by the STV camera will also effectively focus the target on the fibers.

##### 3.1.2. Fiber Centering

In the second fold mirror position, precise target placement on the fiber may be accomplished. Telescope light comes into focus in the plane of the focal plane fiber ferrules. Guide fibers (Section 3.2) are monitored with a second SBIG STV camera while the alignment of the target star is fine-tuned. To image the array of guide fibers, a system of two achromatic doublet lenses is used to demagnify the object plane 3.3 times. When alignment is achieved, the target’s light is centered on the science fiber (Sec. 3.2) and travels to the bench spectrograph. At this point, the auxiliary telescope autoguider (mounted piggyback on the telescope tube) may be engaged if necessary (e.g., for fainter stars) and observing can begin.

##### 3.1.3. Spectral Calibration

In the final fold mirror position, the optical fibers may be illuminated by calibration lamp light. Three wavelength calibration lamps (Neon, Argon, and Xenon) are available as well as a 10 watt Quartz-Tungsten-Halogen (QTH) lamp. These lamps are all independently controlled and illuminate an opal diffusing glass that is in turn imaged onto the plane of the fibers. A system of two achromatic doublets magnifies the opal glass two times and focuses the calibration light at  $f/13.5$  to match the  $f$ /ratio created by the telescope during target observation, and thereby creates the same collimator filling factor at the bench spectrograph.

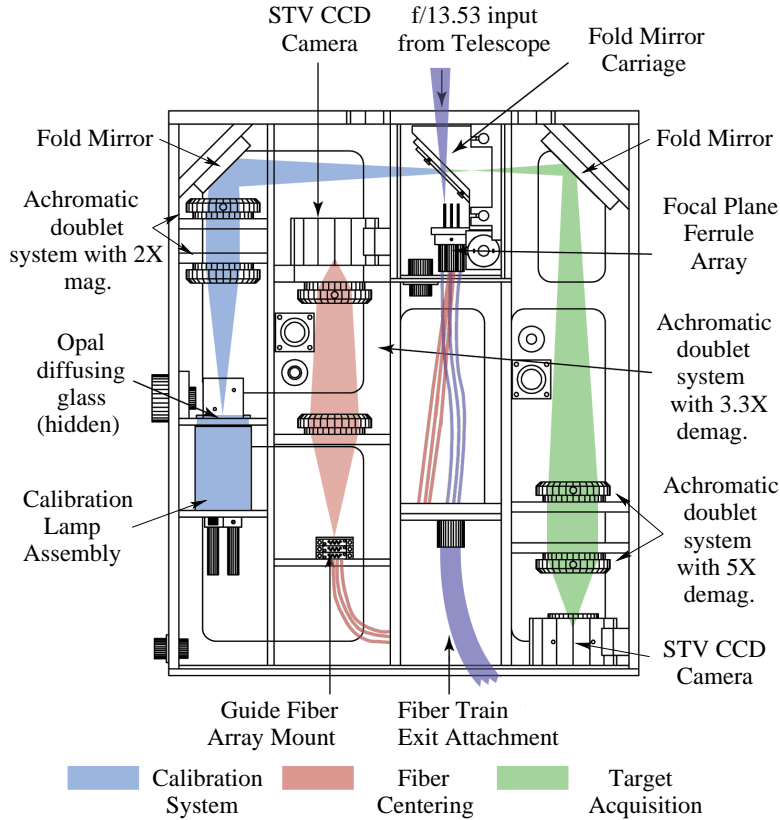


FIG. 2.— Diagram of the interior of the focal plane module.

### 3.2. The Fiber Train

We are using step-index optical fiber with a  $200\ \mu\text{m}$  low OH silica core from Polymicro Technologies (type STU). In the telescope’s  $15.0''/\text{mm}$  focal plane, this fiber diameter corresponds to  $3''$  on the sky, roughly twice the estimated average seeing for the FMO site.

The main length of the fiber train consists of seven redundant, 85 foot long “science fibers” that transmit light from the telescope to the bench spectrograph two floors below the dome room. Although this is a single-object spectrograph, we opted to include seven fibers held in a static array at the focal plane for three reasons. First, while one fiber is collecting stellar light, the “empty” fibers can be used to collect blank sky light for subtraction during data reduction. Using the average of several independent blank-sky spectra decreases the noise contribution of the sky subtraction to the difference spectrum. Second, the extra fibers provide redundancy that may be invaluable in the event that individual science fibers are broken. Finally, use of seven fibers allows the bundling of the full length in a close-pack hexagonal array, which provides extra rigidity and reduces the possibility of fiber tangling.

In the telescope’s focal plane, each science fiber is mounted in a ferrule (Fig. 3) and surrounded closely by 6 short “guide fibers,” the back ends of which are viewed by a CCD camera, similar to the spectrograph design

employed in the Multi-Telescope Telescope (Barry 1996). During target acquisition and exposure, the guide fibers can be monitored for stellar light as a measure of the accuracy of alignment; when each of the guide fibers is equally illuminated by light from the wings of the stellar point spread function, the target star is centered on the array and therefore also the science fiber. In principle, autoguiding of the telescope is possible via frame grabbing of the video feed and evaluating relative fluxes in each guide fiber, as, e.g. with the “Field Orientation Probes” of the National Optical Astronomy Observatory’s Hydra spectrograph (Barden et al. 1993), but this has yet to be implemented. In fact, we have found the telescope to track sufficiently well that manual guiding (using the telescope’s hand paddle) is not an overly onerous task (and, of course, an advantage of fibers over slits is that poor centering only translates to loss of light — not a change in the recorded equivalent “slit function”).

After being cut to length, all fibers were inserted into black teflon tubes with  $460\ \mu\text{m}$  inner diameter to provide a first layer of protection over the cladding as well as to prevent cross-talk. The seven science fibers were then bundled together in a close-pack hexagonal array for their full length and held in place using  $\sim 1\ \text{cm}$  lengths of shrink-wrap tubing spaced at two inch intervals. The spectrograph ends of the science fibers and the CCD ends

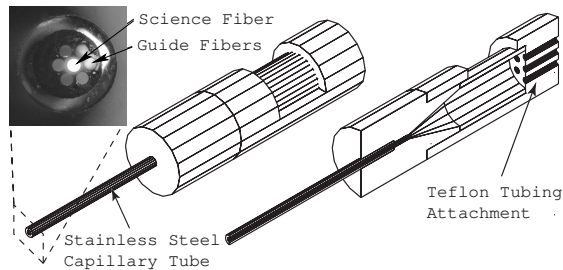


FIG. 3.— The focal plane fiber ferrule shown in isometric projection in full and in cross-section. The teflon tube-encased fibers enter at the base where the teflon tubes are epoxied to the aluminum. The fibers themselves are then brought to a close-pack hexagonal array in the capillary tube extension. In the photo, the central fiber has been back-illuminated. While the fibers in the photo are themselves oriented well with respect to each other, the bundle is off-center within the capillary tube, a fact that is of no consequence to target acquisition.

of the guide fibers were terminated in 1/16" outer diameter stainless steel capillary tubes with the fibers held in place using low-expansion epoxy. The fiber terminations in the telescope's focal plane are somewhat more complicated since each science fiber has to be closely surrounded by its six guide fibers (Fig. 3). For these, the science fibers and surrounding guide fibers were bundled together, coated with epoxy, and allowed to dry before being inserted into capillary tube extensions with larger inside diameters. The bundles were then affixed inside the tubes using more epoxy. The completed science fiber train was fed through a flexible PVC conduit to provide some measure of protection against accidental crushing.

The ferrule ends and encased fibers were polished by hand using jigs that held the stainless steel capillary tubes against abrasive sheets. Six levels of aluminum oxide lapping film ranging from 30 to 0.3  $\mu\text{m}$  grit sizes were used to refine the polish, following the procedure outlined by Barry (1996).

Ideally, one would construct the complete fiber train and then test it to assess the effects of focal ratio degradation (FRD) *prior* to the design of the bench spectrograph. However, the fiber work was very time-consuming and this would have delayed progress. With the desire to expedite the design process, we elected instead to evaluate a 2-meter test fiber length prior to the construction of the actual fiber train. Using the method described by Carrasco & Parry (1993), it was estimated that with the effects of FRD, approximately 90% of the f/13.5 fiber input would exit within an f/5 cone.

We chose to feed the fibers directly from the telescope without any intervening fore-optics. As an alternative, however, one might consider the benefits of using a focal reducer prior to the fiber entrance. It is well established that the fractional FRD in a fiber improves as the focal ratio of the input light is lowered (See Figure 8 of Carrasco & Parry 1993). Furthermore, the degree of FRD in a fiber is strongly affected by the method in which it is terminated and by the quality of the end polish. One might hope to minimize FRD such that for a small input focal ratio, the majority of the light would exit within a similar cone angle. The benefit of reducing the input focal ratio is that the fiber diameter can then be reduced, resulting either in an increase of the spectral resolution

or in a relaxation of the grating angular dispersion requirement and a subsequent effective increase in system throughput. FOBOS as designed meets its resolution and efficiency requirements, so fore-optics were avoided for the sake of cost and simplicity. However, the benefits of fore-optics for other spectrograph designs should be carefully considered.

### 3.3. The Bench Spectrograph

The bench spectrograph (Fig. 4) is mounted on a 4-inch thick optical table that sits on a pneumatically controlled vibration isolator. The seven science fibers are held in a linear array in the science fiber mount assembly, with the light exiting horizontally. An optional 100  $\mu\text{m}$  slit mask can be inserted immediately in front of the fibers to increase resolution at the expense of a nearly 40% throughput loss. By default, however, no mask is used, and the fiber ends themselves define the effective entrance "slit". Following the slit, but still within the science fiber mount, are two slots for optional filters. This location is easily accessible to the observer and allows for the use of modestly sized (1 inch) filters. Due to space restrictions between the spectrograph camera optics and the CCD dewar, it was necessary to place the instrument's shutter at the front of the science fiber mount.

Following the results of the initial FRD testing, we restricted our search for a collimator to optics that were either f/5 naturally or that could be stopped to this f/ratio. Use of an on-axis paraboloidal reflector would have resulted in light loss due to vignetting between the collimator and grating, a negative consequence of using inexpensive reflective optics. This was viewed as unacceptable given our desire to maximize instrument efficiency. Cost considerations and limited off-the-shelf availability prevented us from choosing an off-axis paraboloidal reflector. Ultimately, then, we chose to use a lens for the collimator — a 100 mm diameter, 350 mm focal length achromatic doublet that could be stopped to f/5 with a 70 mm iris diaphragm mask on the collimated side of the beam. The collimator is focused by manually adjusting the micrometer setting on the linear stage that holds the lens mount, while simultaneously viewing the fiber and ferrule ends through a small telescope, focused at infinity, set in the collimated beam.

For the nominal GGSS spectral coverage, dispersion is provided by a 1200 line/mm plane reflectance grating blazed at  $21.1^\circ$  for  $\lambda = 6000\text{\AA}$  in first order. We chose this high groove density to give the necessary spectral range across our 2-inch detector in first order with the camera lens described below. Diffraction gratings with lower groove densities would not give us the desired GGSS spectral range with our collimator/camera combination. In this setup, the angle of incidence on the grating is smaller than the angle of diffraction. This is an unconventional choice that helps to reduce vignetting at the camera aperture since the anamorphic factor reduces the diameter of the diffracted monochromatic beam. Had we chosen to design custom camera optics with a larger aperture, it would have been more beneficial to choose a setup where the incident angle was larger than the diffracted angle. In this case, the anamorphic factor would improve the spectral resolution. Despite this unconventional setup on the FOBOS optical bench, the required spectral resolution is achieved. The grating is housed in

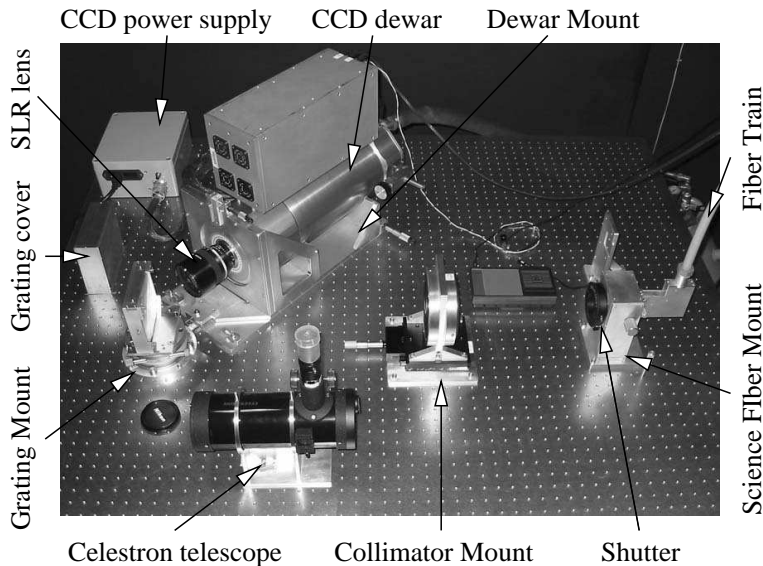


FIG. 4.— The bench spectrograph. The fiber train attaches to the science fiber mount assembly on the right. After a curve in the fibers, light exits horizontally. The CCD and camera rotate on a pivot arm (not visible in this view) to allow a range of collimator-grating-camera angles. The Celestron telescope is used to focus the collimator.

an aluminum structure that sits on a steel rotation stage operated to 1 arcminute accuracy via adjustment of a manual drive with a vernier readout. The grating and grating housing can be easily removed from the rotation stage to allow use of other gratings from the inventory. Set screws in the grating housing allow three-axis rotation of the grating itself so that the spatial alignment of spectra on the CCD can be fine-tuned.

Considering our demagnification requirements as well as the collimated beam diameter, the ideal camera focusing optics would be somewhat faster than  $f/1.25$  with a diameter a bit larger than 70 mm. We were not able to find off-the-shelf optics that met these goals, but instead chose to use a Nikon telephoto 135mm  $f/2.0$  SLR camera lens focused at infinity. The effective lens acceptance diameter is smaller than would be ideal, resulting in vignetting at the edges of the spectrum. The focal length is also longer than desired. However, it is still adequate to meet our resolution goals. Because the optical design of such commercial lenses is proprietary, accurate and detailed modeling of the spectrograph optics could not be accomplished. Performance had to be estimated by assuming a paraxial surface for the camera lens.

The camera lens mounts directly to the front surface of the CCD dewar mount. Although the back focal length of SLR lenses are well established, the back focus of the camera lens must be adjusted slightly for very red and very blue spectral coverage since SLR lenses are not typically designed to be achromatic over a large range of wavelengths.

The dewar mount rides on a steel alignment arm that pivots directly below the center of the front surface of the grating. This swing arm keeps the camera aligned with the grating and allows adjustment of the collimator-grating-camera angle over a wide range. Dewar rotation about the normal to the optical table may be accomplished by adjustment of a micrometer setting and is useful for achieving optimal polychromatic focus when

tilt is present in the spectral focal plane. Dewar rotation about the optical axis may be accomplished by adjusting a second micrometer and is useful for achieving optimal alignment of spectra along CCD pixel rows.

Due to budgetary constraints, the spectrograph had to be designed to work with one of FMO's existing research CCDs — a SITe 2048×2048 array with 24  $\mu\text{m}$  square pixels. With 2000  $\text{\AA}$  of wavelength coverage, the best possible spectral resolution that can be achieved is  $\sim 2 \text{\AA}$  at the Nyquist limit. In order to achieve this, the 200  $\mu\text{m}$  optical fiber core needed to be demagnified by the spectrograph optics by about a factor of 4. Assuming the ability to centroid a single resolution element by a factor of 20 (an extremely conservative assumption, as evidenced by our ability to consistently attain considerably better effective centroiding using our own cross-correlation software), velocity resolutions of  $\sim 5 \text{ km s}^{-1}$  would be attainable if the Nyquist limit were reached. However, the combination of camera and collimator optics chosen give a spectral resolution of  $\sim 4 \text{\AA}$  after anamorphic magnification is considered. Although this meets the velocity resolution goals, an optional 100  $\mu\text{m}$  slit mask may be used just in front of the science fiber output in order to double the resolution to the Nyquist limit at the expense of a nearly 40% throughput loss. The slit is thus useful for maximizing resolution capabilities, but is recommended only for brighter sources.

The specifications of the various bench optics are summarized in Table 1.

### 3.4. The Spectrograph Enclosure

To achieve the highest possible consistency between observations, it is preferable to maintain a steady, controlled environment around the optical table. The air should be still and at a constant temperature throughout the night. Moreover, humidity in Virginia can be a serious problem; condensation can easily develop on optical surfaces if the dew point is not monitored and controlled.

Parameter	Value
Optical fiber core diameter ...	200 $\mu\text{m}$
Collimator focal length .....	350 mm
Collimator effective f/ratio ...	f/5
Grating angle of incidence ....	-2.7°
Grating groove density .....	1200 lines/mm
Grating blaze angle .....	21.1°
Grating blaze wavelength ....	$\sim 6000 \text{ \AA}$
Central diffraction angle .....	47.9°
Total collimator-camera angle	50.6°
Camera effective focal length .	135 mm
Camera effective f/ratio .....	f/2
Spatial demagnification .....	2.59 $\times$
Spectral demagnification .....	1.75 $\times$
Detector dimensions .....	2048 $\times$ 2048
Detector pixel width .....	24 $\mu\text{m}$
Linear dispersion .....	1.0 $\text{\AA}/\text{pixel}$

TABLE 1  
BENCH SPECTROGRAPH OPTICAL COMPONENT SPECIFICATION  
SUMMARY. THESE NUMBERS ARE APPLICABLE TO THE FOBOS  
CONFIGURATION USED FOR THE GGSS.

Finally, because source light levels are so low — especially after passing through a fiber system — sources of extraneous background light need to be eliminated. For these reasons, a special enclosure was constructed for the bench spectrograph on the second floor of the observatory, two floors below the telescope.

The enclosure’s walls and ceiling are six inches thick and filled with fiberglass insulation. A double door entryway leads to an interior coated with flat black, non-fluorescent paint illuminated with incandescent lights. A window-mount air conditioner is set directly into one wall with a framed, well-sealed door that covers it at night. A dehumidifier keeps the humidity at safe levels. In addition, an air cleaner runs continuously during the day to minimize airborne dust. These devices are powered off prior to nighttime observing in order to let the air equilibrate and still.

An environmental monitoring and control system has been designed to maintain appropriate conditions inside the spectrograph enclosure. Two resistance temperature detectors monitor the concrete floor and air temperatures while a humidity sensor measures the air’s water content. These sensors are connected to a National Instruments Field Point distributed I/O network that feeds data to a personal computer in the observatory control room. The PC is running a National Instruments LabView-based program that monitors conditions in the room and can operate the environmental control devices as necessary. During the day, the room may be cooled to match the temperature of the concrete floor. During nighttime observing, the thermal mass of the floor maintains the air temperature reasonably well.

#### 4. DATA CALIBRATION

Data calibration is accomplished using a combination of internal comparison lamp exposures and on-sky observations.

Each night, a set of bias frames is collected, combined, and subtracted from each data frame. Flat field images are created by placing an opal diffusing glass in one of the two filter slots in front of the fiber output in the bench spectrograph. The QTH lamp is used to illumi-

nate the opal glass with bright, diffuse light. Since the opal glass is out of focus relative to the collimator, it acts as a good flat source useful for removing pixel-to-pixel variations in the spectral images. These frames are referred to as “milky flats”, following the convention used with the Hydra bench spectrograph at the Cerro Tololo Inter-American Observatory.

In most cases, multiple science fibers will be used to collect background sky emission while the central science fiber collects light from the target star. In order to combine the multiple sky spectra effectively, relative throughput differences between them need to be estimated and taken into account prior to subtraction from the stellar spectrum. This is best accomplished by observing the daytime or twilight sky. The uniform illumination over all fibers in the telescope’s focal plane is very good for estimating fiber throughput variations. Once throughput variations are removed, sky spectra are combined in wavelength space after dispersion correction with reference to calibration lamp exposures.

One-dimensional spectra are extracted from the images with reference to apertures determined by tracing the paths of spectra created by the QTH lamp. A one-second exposure suffices to produce broadband continua bright enough to map out the traces of each fiber’s spectrum across the detector.

Once extracted to one dimension, spectra may be calibrated to determine the wavelength-to-pixel mapping. Three wavelength calibration lamps are available: Neon, Argon, and Xenon. Each are controlled independently, a necessity since the Neon lamp is considerably brighter than the others. Typical exposure lengths for wavelength calibration are 60 seconds for Xenon and Argon and 1 second for Neon. In that time, enough bright emission lines appear to span the wavelength ranges of interest so that good pixel/wavelength calibrations may be determined. It appears that the spectrograph is stable enough that wavelength calibration spectra need only be collected once per night (see Section 6.2).

#### 5. DATA REDUCTION

Data are reduced using a combination of native and locally written IRAF (Tody 1986) tasks as well as a radial velocity cross-correlation program written at the University of Virginia.

An IRAF package called FOBOS has been written to streamline and partially automate data reduction. After median combination of a set of bias frames, all data and calibration frames are bias-subtracted, overscan-corrected, and trimmed. A flat field image is then generated by combining the milky flat frames and dividing out the large-scale image structure to leave only pixel-to-pixel variations. The flat field is then divided into the remaining frames. Next, QTH lamp and daytime sky exposures are extracted using the IRAF APALL routine. The latter are used to estimate the fiber-to-fiber throughput differences, which are useful later during sky subtraction. If target observations have been split up into multiple, adjacent exposures (recommended to facilitate removal of cosmic rays), these are then combined at this point. Finally, a new routine called FOBOSEXT is run that extracts the wavelength calibration and object images to 1-dimensional spectra, determines the wavelength-to-pixel mapping of the arc lamp exposures by interactively

prompting the user to identify emission lines in the arc lamp spectrum, dispersion corrects the object spectra, and subtracts the background sky emission after combining spectra obtained from the blank sky fibers. A sample spectrum is shown in Figure 5.

Following these reductions, radial velocities may be estimated by cross-correlating the extracted, wavelength-calibrated target spectra against a set of radial velocity standard stars of similar spectral type. This is executed using a MATLAB code written locally by M. Garvin, and following the general precepts for filtered cross correlation described by Majewski et al. (2004).

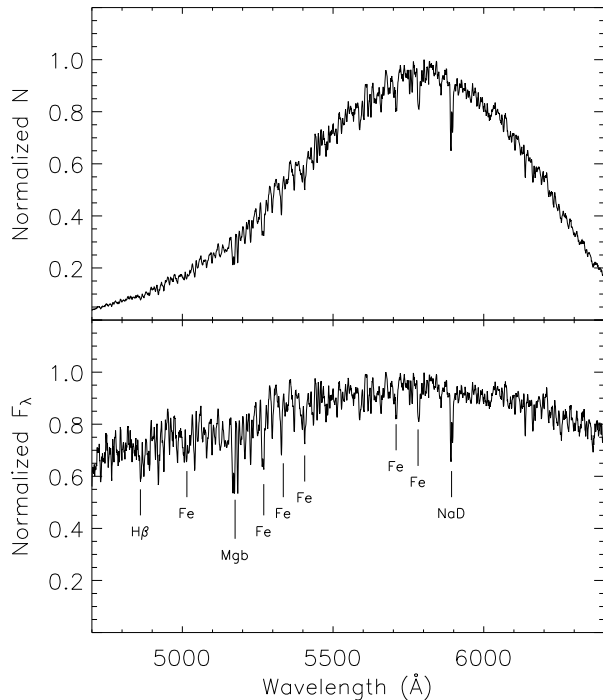


FIG. 5.— FOBOs spectrum of HD 26162, a K1 giant with  $[\text{Fe}/\text{H}] = -0.02$ . The upper panel shows normalized counts in the raw spectrum while the lower panel shows the normalized, flux-calibrated spectrum. Many useful absorption features are visible including  $\text{H}\beta$  (4861Å), the  $\text{MgB}$  triplet (5167-5184Å), the  $\text{Na I}$  doublet, and a multitude of  $\text{Fe}$  lines. In addition, the  $\text{MgH}$  band is present near 5150Å, but is not obvious in the spectrum of this low surface gravity star.

## 6. PERFORMANCE

### 6.1. Throughput

The throughput of the FOBOs + telescope system was estimated by observing the spectrophotometric flux standard star Feige 110 under photometric conditions on UT 2003 November 29. Following the standard CCD reductions and spectral extraction described above, the accumulated counts in the observed spectrum were compared to the expected number calculated from the Feige 110 spectrophotometric data given in the IRAF IRSCAL database. This database gives the calibrated, monochromatic AB system magnitudes for the standard star in a series of either 49 Å or 98 Å bins. These magnitudes were converted to predicted counts at the telescope’s entrance aperture using the formula:

$$DN(\text{ADU}) = 3.68 \times 10^{-20} \times 10^{-0.4m_{AB}} \times 10^{-0.4k_{\lambda} \times X} \times \frac{c \times 10^8}{\lambda(\text{Å})^2} \times \frac{\lambda(\text{cm})}{hc} \times \pi(r_{\text{prim}}^2 - r_{\text{sec}}^2) \times \frac{Exp}{Gain} \times \Delta\lambda_{\text{bin}}(\text{Å}) \quad (1)$$

where  $m_{AB}$  and  $k_{\lambda}$  are the calibrated magnitude and atmospheric extinction, respectively, in the wavelength bin centered on  $\lambda$  with width  $\Delta\lambda_{\text{bin}}$ ,  $X$  is the airmass of the observation,  $c$  is the speed of light in  $\text{cm sec}^{-1}$ ,  $h$  is Planck’s constant in  $\text{erg s}$ ,  $r_{\text{prim}}$  is the radius of the primary telescope aperture,  $r_{\text{sec}}$  is the radius of the telescope’s secondary mirror cell,  $Exp$  is the exposure time of the observation, and  $Gain$  is the CCD gain in electrons/ADU. The resulting expected counts in each wavelength bin were then divided into the observed counts in the same bin to produce the efficiency curve in Figure 6.

At the time that these efficiency data were collected, the telescope’s mirrors had not been aluminized for more than four years. Due to persistent problems with humidity and condensation at the site combined with the advanced age of the mirror coatings, we expect that the telescope’s efficiency has adversely affected the total system efficiency as plotted in Figure 6. In addition, seeing conditions were somewhat worse than average for the FMO site, so that performance here may be underestimated. Moreover, the blue response of the mirror coatings has likely decayed more quickly than the red response. Therefore, we expect that this efficiency estimate does not accurately reflect the actual performance of the spectrograph itself. Following the next scheduled re-aluminization of the telescope mirrors, a significant improvement in the overall throughput, especially at bluer wavelengths, is expected. Overall efficiency will also improve with better seeing. Thus, Figure 6 gives a lower limit to the performance of FOBOs.

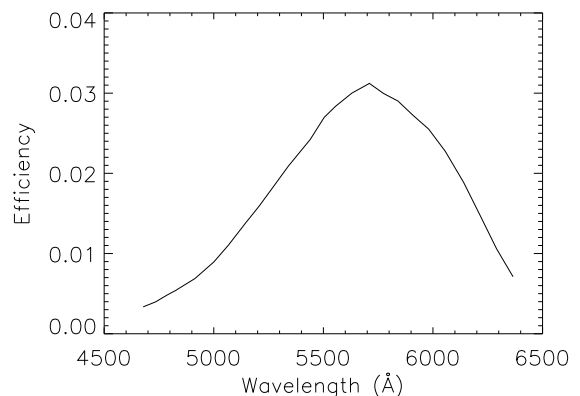


FIG. 6.— Throughput vs. wavelength for the telescope + FOBOs system in the GGSS setup. The efficiency of FOBOs alone should be higher because we expect considerable contribution to the reduced efficiency (especially at shorter wavelengths) by the telescope mirrors that had not been aluminized for several years at the time these data were collected.

It is of more practical use to explore the instrument’s sensitivity in terms of the achievable signal-to-noise ratio

(S/N) as a function of source magnitude. A number of calibrating stars covering a range of magnitudes were observed on UT 2003 October 31 and UT 2003 November 29. All were reduced using the methods described in Section 5 and the resulting spectra were evaluated to determine their peak S/N. The results are plotted in Figure 7, which shows the effective S/N that would be achieved for each star in one second of exposure (note, however, that the actual exposures used to perform this evaluation were longer than one second). A linear fit to the data was derived with equal weighting for all 37 points. Based on this fit, exposure times may be predicted for any source  $V$  magnitude and target S/N (Fig. 8).

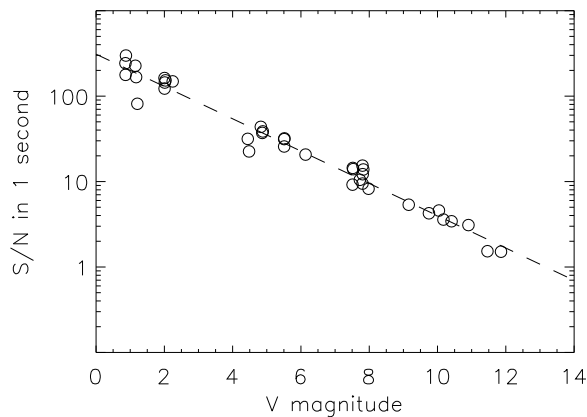


FIG. 7.— Peak signal to noise ratio per pixel generated in one second at one airmass. This represents a practical view of the instrument’s sensitivity.

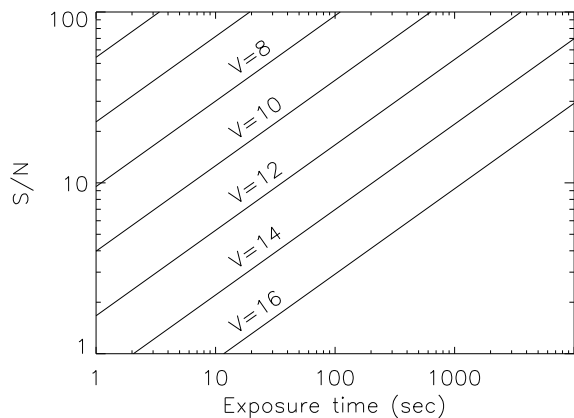


FIG. 8.— Lower limit to the predicted signal to noise ratio vs. exposure time for different apparent magnitudes.

## 6.2. Velocity Measurement Accuracy and Stability

FOBOS was built, in part, to provide stable radial velocity measurements. On UT 2003 November 29, 26 spectra of radial velocity standards were collected, several of which were repeat observations of individual stars. The data were then reduced using two different methods.

In the first method, each spectrum was extracted with an aperture referenced to a QTH lamp exposure taken

immediately after the object exposure. The spectra were then wavelength-calibrated using arc lamp spectra collected immediately after the adjacent QTH exposures. In the second method, all spectra were extracted and wavelength-calibrated using only a single QTH and arc lamp exposure pair taken at the beginning of the night.

Within each of these two groups, the spectrum of each star was cross-correlated with all of the others, producing 25 individual measurements of each star’s radial velocity. Each star’s 25 velocity measurements were then averaged and a standard deviation was calculated. The mean standard deviations reported for each star’s velocity measurements were  $2.3 \text{ km sec}^{-1}$  and  $2.8 \text{ km sec}^{-1}$  for methods 1 and 2, respectively. For bright ( $V < 8$ ) stars, this appears to be the limit of the instrument’s velocity precision for a single spectrum produced with the 1200 line/mm grating while observing without the optional aperture slit, and is well within the original design goals.

For spectra reduced using method 1, the mean velocity error (defined as  $\bar{v}_{err} = N^{-1} \sum |v_{lit} - v_{obs}|$ , where  $v_{obs}$  is the measured velocity and  $v_{lit}$  is the velocity taken from the Astronomical Almanac (U. S. Naval Observatory & Royal Greenwich Observatory 2001)) and dispersion about the mean was  $\bar{v}_{err} = 1.5 \pm 1.2 \text{ km sec}^{-1}$  while method 2 resulted in  $\bar{v}_{err} = 2.0 \pm 1.3 \text{ km sec}^{-1}$  (note that these numbers do not take into account the uncertainties inherent in the published standard velocities, some of which are as high as  $0.5 \text{ km sec}^{-1}$ ). Thus, the systematic errors are small. The distribution of measurement errors is shown in Figure 9. Based on these numbers, it appears that the results one gets from using only a single set of calibration lamp exposures at the beginning of the night are only marginally worse than the results obtained from taking many calibration frames throughout the night. For observing programs that can tolerate the small impact to velocity uncertainties, collecting only one set of calibration frames will result in a significant improvement in observing efficiency.

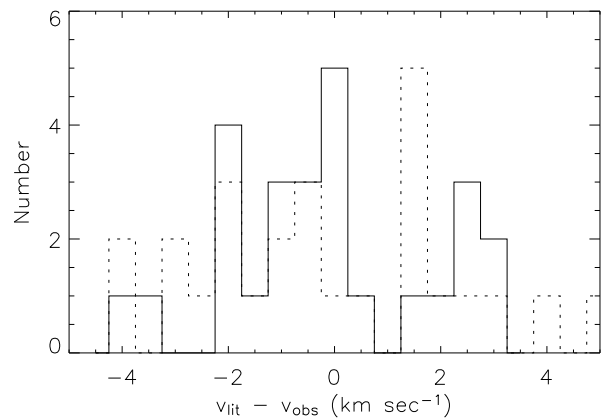


FIG. 9.— Errors in velocity measurements for 26 radial velocity standard star observations reduced using two separate methods. The solid and dotted lines correspond to the reductions using methods 1 and 2, respectively (See text of Section 6.2).

7. SCIENCE AND FUTURE WORK

FOBOS was commissioned in September 2003 and is now being used for scientific research. Several projects are underway and planned for the immediate future.

The northern hemisphere spectroscopic GGSS observing has already begun. As part of this program, several thousand candidate metal-poor K giants in the Galactic halo will be observed to further confirm their suitability as members of the *SIM* Astrometric Grid, required to establish the positional reference frame for that mission. In addition to providing necessary support for *SIM*, however, the GGSS will be a unique catalog of low-metallicity K giants suitable for exploring the structure of the Galactic halo. GGSS observing in the southern hemisphere has already yielded interesting, serendipitous results such as the discovery of kinematic evidence for the presence of a tidal structure associated with the Sagittarius (Sgr) dwarf galaxy (Kundu et al. 2002).

Work is also underway to measure the contribution of dark matter to the local Galactic disk mass density through the measurement of the density and kinematics of a population of K giant tracers in the direction of the North Galactic Pole (Crane 2004). Spectroscopic observations and determinations of tracer star velocities were in part executed using FOBOS during Spring 2004.

FOBOS is being used to characterize the occurrence of emission lines within the complete B-star populations of an age-selected sample of open clusters to a distance of 1 kpc in a study of the evolutionary status of Be stars. Red spectra including the H $\alpha$  6563Å and He I 6678Å lines can be obtained for stars as faint as  $V = 13$ , reaching the latest B spectral types missing in previous studies and providing positive identification of Be stars with weak emission that are difficult to detect using narrow band photometry.

Finally, FOBOS will be used to measure the radial velocities of M giant candidate members of both the Sgr tidal tail system (e.g., Majewski et al. 2003) and the Galactic Anticenter Stellar Stream (e.g., Yanny et al. 2003; Crane et al. 2003) to further constrain their orbits and to gain insight into the nature of the Milky Way's gravitational potential.

We thank James Barr and Charles Lam for lending their technical skills and expertise, without which this project would have been considerably more difficult. David McDavid, Howard Powell, Robert Rood, and Kiriaki Xilouris each provided support at various stages of the project. We thank Megan Kohring for her assistance in constructing the fiber train. William Kunkel, Di Harmer, Robert Jones, Robert O'Connell, Ray Ohl, Neill Reid, and John Wilson provided insightful comments during useful discussions. We thank Matthew Garvin for providing software that aided our analyses. Finally, we thank Daniel Fabricant and the anonymous referee for editorial comments that helped to improve this paper. This work has been supported by NASA/JPL grant 1222563 as part of the NASA *Space Interferometry Mission* and a Cottrell Scholar Award from The Research Corporation. This research was also partially supported by the The F.H. Levinson Fund of the Peninsula Community Foundation and a David and Lucile Packard Foundation fellowship to S.R.M. J.D.C. has been aided by a Grant-in-Aid of Research from the National Academy of Sciences, administered by Sigma Xi, The Scientific Research Society, and by an Aerospace Graduate Research Fellowship, administered by the Virginia Space Grant Consortium.

REFERENCES

Barden, S. C., Armandroff, T., Massey, P., Groves, L., Rudeen, A. C., Vaughn, D., & Muller, G. 1993, in ASP Conf. Ser 37, *Fiber Optics in Astronomy*, II, ed. P. M. Gray (San Francisco: ASP), 185

Barry, D. J. 1996, Ph.D. Thesis, Georgia State University

Carrasco, E. & Parry, I. R. 1993, in ASP Conf. Ser 37, *Fiber Optics in Astronomy*, II, ed. P. M. Gray (San Francisco: ASP), 392

Crane, J. D., Majewski, S. R., Rocha-Pinto, H. J., Frinchaboy, P. M., Skrutskie, M. F., & Law, D. R. 2003, *ApJ*, 594, L119

Crane, J. D. 2004, Ph.D. Thesis, University of Virginia

Kundu, A. et al. 2002, *ApJ*, 576, L125

Majewski, S. R., Skrutskie, M. F., Weinberg, M. D., & Ostheimer, J. C. 2003, *ApJ*, 599, 1082

Majewski, S. R., et al. 2004, *AJ*, 128, 245

Patterson, R. J., & Ianna, P. A. 1991, *AJ*, 102, 1091

Patterson, R. J., et al. 2001, in IAU Colloq. 183, *Small Telescope Astronomy on Global Scales*, eds. W. P. Chen, C. Lemme, & B. Paczyński (ASP Conf. Ser. 246; San Francisco: ASP), 246

Tody, D. 1986, *Proc. SPIE*, 627, 733

U. S. Naval Observatory & Royal Greenwich Observatory 2001, *The Astronomical Almanac for the year 2003*, Washington: U.S. Government Printing Office (USGPO) and London: The Stationery Office, 2001.

Yanny, B. et al. 2003, *ApJ*, 588, 824